ELSEVIER

Marine Geology 190 (2002) 581–589

MARINE GEOLOGY
INTERNATIONAL JOURNAL OF MARINE GEOLOGY, GEOCHEMISTRY AND GEOPHYSICS

www.elsevier.com/locate/margeo

Fast reconnaissance of carbonate dissolution based on the size distribution of calcareous ooze on Walvis Ridge, SE Atlantic Ocean

Jan-Berend W. Stuut[a,b,*], Maarten A. Prins[c], J.H. Fred Jansen[a]

[a] *Royal Netherlands Institute for Sea Research (NIOZ), P.O. Box 59, 1790 AB Den Burg, The Netherlands*
[b] *Faculty of Earth Sciences, Utrecht University, P.O. Box 80.021, 3508 TA Utrecht, The Netherlands*
[c] *Faculty of Earth Sciences, Vrije Universiteit, De Boelelaan 1085, 1081 HV Amsterdam, The Netherlands*

Received 11 April 2002; received in revised form 22 May 2002; accepted 14 July 2002

Abstract

We present a new index of carbonate fragmentation based on the size distribution of bulk sediments in core MD962094 from Walvis Ridge (SE Atlantic Ocean). The carbonate fragmentation index is constructed by taking a ratio of the two coarsest fractions in the grain size distributions of the bulk calcareous ooze. The coarsest two fractions (25–90 µm and > 90 µm) of the bulk sediments consist primarily of complete shells and fragments of adult foraminifera shells, and juvenile foraminifera shells and fragments, respectively. The ratio of the proportions of the two fractions is interpreted as a measure of fragmentation of the foraminifera shells caused by carbonate dissolution. Downcore changes in our carbonate fragmentation index compare very well with those in the coarse-carbonate fragmentation index in sediments from a nearby core on Walvis Ridge. The latter commonly used fragmentation index is defined as a ratio of foraminifera fragments over whole foraminifera in the > 150-µm fraction as seen with a light microscope. Fragmentation is relatively high during glacial stages and relatively low during interglacial stages during the last 300 kyr, caused by the combined effect of wind-driven upwelling of corrosive water and increased production of organic matter, decreasing the preservation potential of carbonates both during and after deposition. The carbonate fragmentation index we present here provides a precise and fast method to establish a downcore fragmentation record. It can be applied to bulk sediments that are carbonate-rich ($CaCO_3 > 68\%$) and to all other deep-marine sediments of which the grain size distribution of the carbonate-free fraction is available.

Keywords: carbonate fragmentation; carbonate dissolution; laser diffraction particle sizer; grain size distribution; upwelling

1. Introduction

The lysocline and calcite compensation depth are boundaries in the present ocean below which carbonate dissolution starts and below which dissolution exceeds deposition of carbonate, respectively. The position of these boundaries is mainly

* Corresponding author. Present address: Research Center Ocean Margins, Bremen University, P.O. Box 330440, 28334 Bremen, Germany.

E-mail address: jbstuut@rcom-bremen.de (J.-B.W. Stuut).

PII: S0025-3227(02)00478-4

a result of the interplay between the carbonate saturation of deep waters and organic carbon production in the surface waters. (Bramlette, 1961; Parker and Berger, 1971; Broecker and Takahashi, 1980; Emerson and Bender, 1981; Le and Shackleton, 1992; Kucera et al., 1997). Temporal changes in carbonate dissolution therefore, can be used to reconstruct changes in the position of the lysocline and carbonate compensation depth through time (Peterson and Prell, 1985a,b; Farrell and Prell, 1989; Le and Shackleton, 1992).

Carbonate dissolution has been inferred in various ways, e.g. by looking at species-selective dissolution of planktonic foraminifera (Arrhenius, 1952; Berger, 1968; Parker and Berger, 1971), percentage of planktonic foraminiferal fragments and the percentage of benthic foraminifera relative to the total number of foraminiferal remains (Parker and Berger, 1971; Berger, 1973, 1979; Thunell, 1976; Peterson and Prell, 1985b; Schmidt, 1992), shell thickness of single foraminiferal species of a specific size (Lohmann et al., 1999; Dittert and Henrich, 2000; Huber et al., 2000), coarse carbonate fraction (Bassinot et al., 1994; Broecker and Clark, 1999), and $CaCO_3$ content of the sediments (Farrell and Prell, 1989, 1991; Naidu et al., 1993).

On the basis of the coarse carbonate fraction (>63 μm), Broecker and Clark (1999) reconstructed $CO_3^=$ ion concentrations for the late Quaternary ocean with a very high accuracy. Their study indicates that a high-precision estimate of carbonate dissolution can be obtained in a relatively simple way. However, the construction of their and most other dissolution indicators is rather labor intensive as it involves wet-sieving and subsequent microscopic observation and enumeration of various size fractions.

We present a new method that allows the establishment of a carbonate fragmentation record on the basis of the size distribution of calcareous ooze. As a case study we analyzed the bulk sediments from Walvis Ridge, SE Atlantic Ocean. Walvis Ridge is a northeast–southwest volcanic ridge, blanketed with carbonate ooze, that rises on average 2000 m above the surrounding sea floor. Sedimentation in this part of the SE Atlantic is controlled by coastal upwelling off Namibia and South Africa. The tradewind-driven upwelling determines primary productivity in the surface waters, thereby also controlling the rain rate of both carbonate shells and organic carbon to the sea floor. The upwelling intensity is related to both atmospheric and oceanic circulation in the area, and has been studied extensively (e.g. Wefer et al., 1996; Fischer and Wefer, 1999). The dominant lithology of core MD962094 is foraminifer nannofossil ooze. Size measurements were carried out on a laser diffraction particle sizer, allowing a fast and high-precision analysis of the sediment size distributions. The carbonate fragmentation index is constructed by taking a ratio of the two coarsest fractions in the grain size distributions of the bulk calcareous ooze. The coarsest two fractions (25–90 μm and >90 μm) of the bulk sediments consist primarily of juvenile foraminifera shells and fragments, and complete shells and fragments of adult foraminifera shells, respectively. The ratio of the proportions of the two

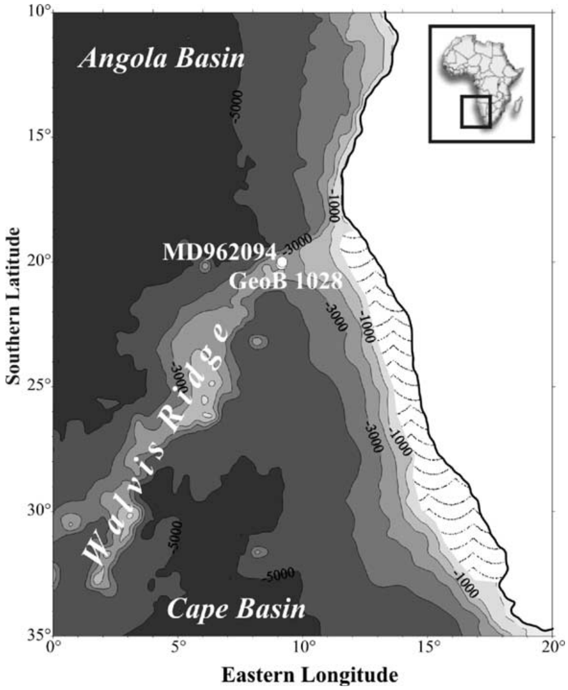

Fig. 1. Location of cores MD962094 and GeoB1028-5 in the SE Atlantic Ocean. Bathymetry is shown in contour intervals of 1000 m. Wavy lines indicate zone of wind-driven coastal upwelling.

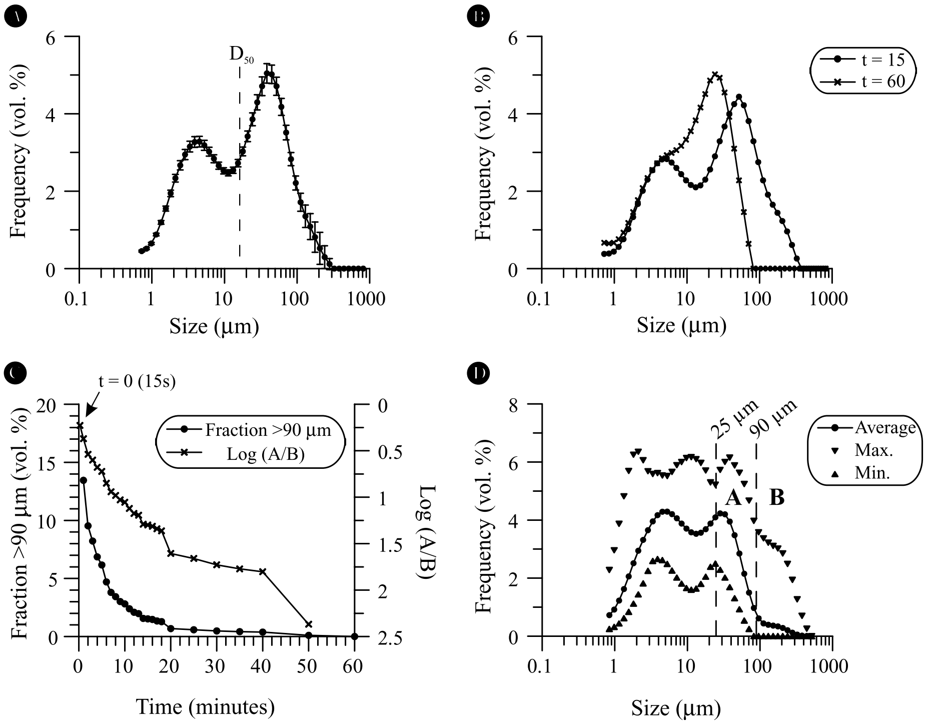

Fig. 2. (A) Reproducibility of the size analyses ($n=9$) tested for sample 56 (MH, 56 cm core depth). D_{50} (median size) = 16.34 µm ± 1.87. (B) Disintegration of foraminifera shells in sample 56 due to ultrasonic dispersion causes a decrease in the size distribution. (C) Decrease of the > 90 µm fraction in sample 56 through time and resultant effect on the (log)-ratio of the coarsest two fractions from the size distributions. (D) Sample statistics of all 276 samples. The boundaries between the coarsest two fractions A and B are indicated with dashed lines.

fractions is interpreted as a measure of fragmentation of the foraminifera shells caused by carbonate dissolution. This new proxy for carbonate fragmentation is validated by comparison with an independent record of foraminifer fragmentation obtained from a core retrieved at about the same location (Fig. 1).

2. Materials and methods

Core MD962094 was recovered from Walvis Ridge at 19°59,97 S, 9°15,87 E and 2280 m water depth. The core is 30.75 m long and covers the last ~650 kyr. The sedimentology and further characteristics of the core are given by Bertrand et al. (1996), the stratigraphy and age model by Stuut (2001) and Stuut et al. (2002). The upper 4.5 m of the core was sampled at 2-cm intervals, the rest of the upper 15 m, which span the last 300 kyr, at 5-cm intervals, for size analyses.

Size analyses of the bulk sediments were carried out with a Malvern Instruments Mastersizer S, using a lens with 300-mm focal length. The measured size distributions were analyzed from 0.73–814 µm. A sample of ~500 mg was suspended in demineralized water by stirring. A subsample was taken from this suspension with a 10-ml pipette and introduced into the sample cell of the laser particle sizer. All samples were suspended in the sample cell by stirring and ultrasonic dispersion for 15 s before analysis.

Reproducibility of the laser particle sizer measurements was tested by multiple analyses ($n=9$) of one sample and appeared to be high (Fig. 2A). The carbonate-rich sediments contain large amounts of foraminifera shells that break because of the ultrasonic dispersion, thereby altering the size distribution dramatically (Fig. 2B). The initial mode at 52 μm in the size distribution at $t=0$ shifts to 24 μm after 60 min. This effect is greatest in the coarser size fractions. The lower plot in Fig. 2C shows the rapid decrease of the proportion >90 μm through time. The size distribution changes most dramatically during the first few min of ultrasonic dispersion. However, ultrasonic dispersion is necessary to prevent the formation of aggregates in the suspension. Therefore, to minimize physical fragmentation of the foraminifera shells before analysis and yet to ensure suspension, we chose to expose the samples to exactly 15 s ultrasonic dispersion prior to the measurements. Subsequently the size distributions of all samples ($n=276$) were measured (Fig. 2D).

3. Size distributions of foraminifer ooze

The average size distribution of the bulk sediments from core MD962094 is polymodal with clear modes at about 5 μm, 30 μm and a small mode at >100 μm (Fig. 2D). Fig. 3A,D shows two extreme size distributions of samples from the Middle Holocene (MH; sample 56) and the Last

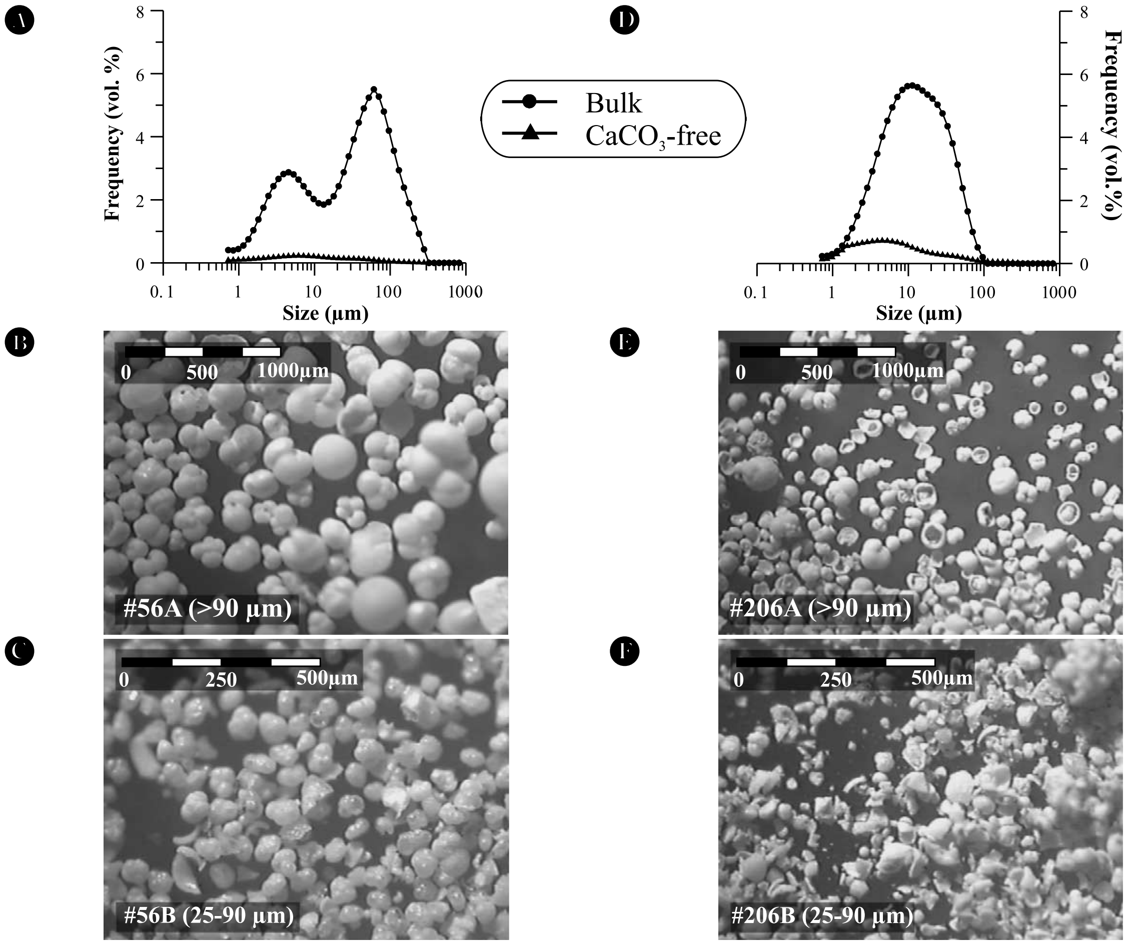

Fig. 3. (A) Size distribution of sample 56 (MH, 56 cm core depth). Size distribution of the carbonate-free fraction is plotted for $CaCO_3 = 88\%$. (B,C) Photos of sample 56. Samples were fractionated into the fractions of which modes are observed in the size distributions using sieves of 25 μm and 90 μm. (D) Size distribution of sample 206 (LGM, 206 cm core depth). Size distribution of the carbonate-free fraction is plotted for $CaCO_3 = 76\%$. (E,F) Photos of fractions A and B of sample 206.

Glacial Maximum (LGM; sample 206), respectively. Next to the grain size distribution of the bulk samples, the distributions of the carbonate-free sediment fractions have been plotted, calculated for 88% and 76% $CaCO_3$, respectively. These figures show that potential disturbance of the bulk size distribution by the terrigenous sediment fraction is negligible due to its low contribution to the grain size distributions caused by the high calcium-carbonate contents. Hence, the bulk sediment size distribution may be used to draw conclusions about the size of the carbonate fraction of the foraminifer nannofossil ooze from Walvis Ridge.

The three modes in the size distributions at 5 μm, 30 μm and 170 μm are mainly attributed to coccoliths, juveniles and small fragments of foraminifera shells, and adult foraminifera shells and large fragments, respectively. Here we consider the two coarsest modes to infer a carbonate fragmentation index. We defined fraction A as 25–90 μm, and fraction B as >90 μm, based on the shape of the maximum size distribution curve (Fig. 2D). The foraminifera shells in fraction A (25–90 μm) from sample #56 (MH) are predominantly complete, only a few shells are broken (Fig. 3B). Fraction B (>90 μm) of the same sample shows more fragments, but complete foraminifera shells prevail in this fraction too (Fig. 3C). Sample #206 (LGM) shows significantly more broken foraminifera shells, both in fraction A and fraction B (Fig. 3E,F). These photographs clearly illustrate that the disintegration of the foraminifera shells has occurred along the edges of the chambers.

4. Carbonate fragmentation index

We defined a carbonate fragmentation index as the (log)-ratio of the relative abundances of the fractions A and B (25–90 μm and >90 μm, respectively). The downcore fragmentation index record is plotted versus age in Fig. 4C. This figure shows that interglacial periods are marked by relatively low values of the index, indicating low fragmentation, and glacial periods are marked by relatively high values of the index, indicating high fragmentation. Reproducibility of the fragmentation index could only be determined for sample #56 since sample #206 does not have size fractions >90 μm (Fig. 3D). Multiple analysis ($n=9$) of the (log)-ratio determined in sample #56 resulted in an error bar of 0 ± 0.25, meaning that the variation observed in Fig. 4C is significant.

An important prerequisite of our method is that the size distribution of the foraminifera in the considered size ranges remains constant through geological history. The foraminiferal assemblages in Late Quaternary Walvis Ridge sediments contain predominantly subtropical planktonic foraminifera with abrupt intervals, mainly during glacial periods, of very high abundances of *Neogloboquadrina pachyderma* (s), attributed to periods of enhanced upwelling (Schmidt, 1992; Little et al., 1997; Ufkes et al., 2000). Because *N. pachyderma* (s) is known as a relatively small species, faunal changes might affect the foraminiferal size distribution and thus, the carbonate fragmentation index. However, this is not the case since the average size of adult *N. pachyderma* (s) is >200 μm (Peeters et al., 1999). Any change in the foraminifera size >100 μm will have little effect on our fragmentation index since all change will occur within fraction B (>90 μm) of our fragmentation index.

Little is known about the influence of changes in the reproductive cycles on the ratio of juvenile and adult foraminifera (Brummer and Kroon, 1988; Peeters et al., 1999). However, the effects on the size distribution that these changes may have, may play a role in an area subject to large changes in primary productivity caused by changes in upwelling intensity. Kroon and Darling (1995) found that the size distributions of foraminifera did change on a glacial/interglacial time scale in the Arabian Sea. These changes, however, all took place in the >280 μm size ranges and, therefore, will not have an effect on our fragmentation index.

Besides, from microscopic studies of the two fractions (Fig. 3) we conclude that fragmentation is the dominant process controlling the size of the bulk sediments in the Walvis Ridge area. We therefore state that the (log)-ratio of the

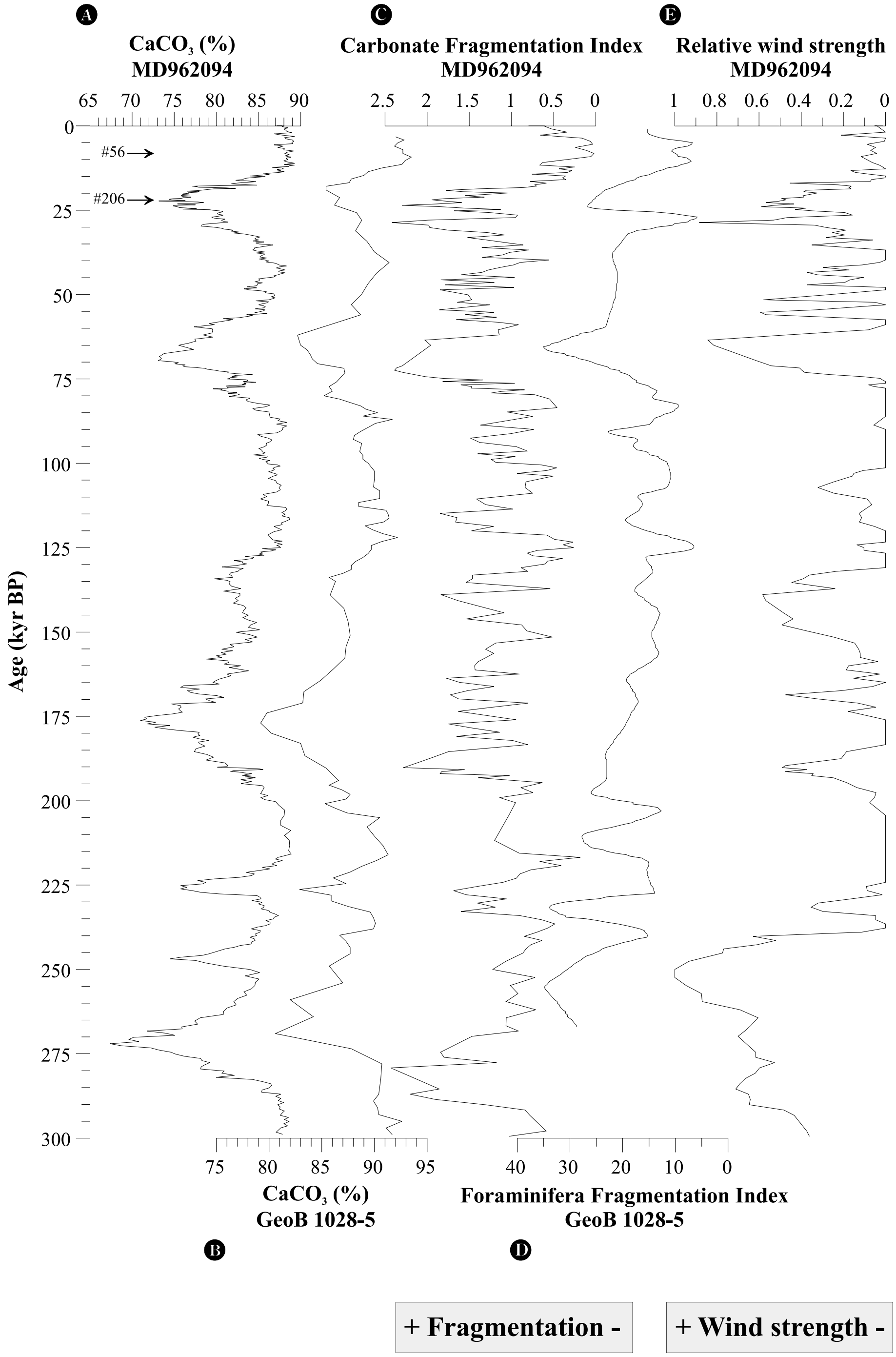
A
CaCO3 (%)
MD962094
C
Carbonate Fragmentation Index
MD962094
E
Relative wind strength
MD962094
#56
#206
Age (kyr BP)
CaCO3 (%)
GeoB 1028-5
B
Foraminifera Fragmentation Index
GeoB 1028-5
D
+ Fragmentation -
+ Wind strength -

two coarsest fractions of the size distributions of the bulk sediments from core MD962094 can be interpreted as a carbonate fragmentation index.

5. Carbonate dissolution, upwelling and tradewind intensity

Walvis Ridge sediments contain large amounts (65–95%) of calcium-carbonate (Embley and Morley, 1980; Diester-Haaß, 1985; Schmidt, 1992). The combination of late Quaternary changes in primary production and dissolution causes the calcium-carbonate content to change from 68 to 94% during the last 300 kyr in cores MD962094 and GeoB 1028-5 (Fig. 4A,B, from Stuut, 2001, and Schmidt, 1992, respectively). Core GeoB 1028-5 lies within 7 km of core MD962094 (Fig. 1). The two cores can be correlated very well on the basis of their planktonic foraminifera $\delta^{18}O$ and bulk chemistry records (Stuut, 2001, chapter 2). The downcore variations in the carbonate fragmentation indices (Fig. 4C,D) show a similar pattern as the $CaCO_3$ records from the two cores. The fragmentation curve of the nearby core GeoB 1028-5 was established using a ratio of the amount of fragments of foraminifera shells over whole foraminifera shells in the >150 μm fraction (Schmidt, 1992, Fig. 4D). The two carbonate fragmentation records (Fig. 4C,D) show similar downcore variations, which confirms our interpretation of the size distribution of the bulk sediments as a measure of fragmentation. The downcore variations in fragmentation of the foraminifera shells in core GeoB 1028-5 are attributed to changes in dissolution owing to changes in the tradewind-driven upwelling intensity (Schmidt, 1992). The upwelling affects carbonate preservation in two ways. Firstly the cold upwelling waters are strongly undersaturated in calcium-carbonate, causing dissolution of the foraminifera shells settling through the water column and on the sea floor. Secondly, the nutrient-rich waters favor productivity in the surface waters, causing high fluxes of organic matter to the sea floor, resulting in high CO_2 levels, lowering the pH of the bottom waters and enhancing carbonate dissolution (Barth et al., 1939; Berger, 1970; Kucera et al., 1997). Although dissolution in the water column cannot be neglected (Berger, 1970), post-depositional dissolution is thought to have the greatest effect on carbonate fragmentation (Berger, 1979; Conan et al., 2002). The relation between wind-driven upwelling and carbonate dissolution is also shown by the comparison of a proxy record for changes in the tradewind intensity (Stuut et al., 2002) and our carbonate fragmentation index record (Fig. 4B). The fragmentation index and the wind-strength record show a good correlation during the last 235 kyr, except from 215–205 kyr BP (Fig. 4C,E). Also from 280–235 kyr BP the correlation is not so obvious. The differences between the two records may result from the fact that upwelling is not always only wind induced, and also depends on the quality of the upwelled water influenced, for example, by the advection of Antarctic Intermediate and Bottom Waters (Ufkes et al., 2000). Besides, changes in the tradewind zonality may also influence upwelling intensity (Little et al., 1997).

The photographs shown in Fig. 3 clearly illustrate that the disintegration of the foraminifera shells occurs along the edges of the chambers of the foraminifera. Especially Fig. 3E shows the separation of individual chambers of the foraminifera. We attribute this disintegration of the foraminifera shells to carbonate dissolution since foraminifera shells are most vulnerable at the

Fig. 4. (A) $CaCO_3$ (%) record of core MD962094, derived from corescanner data (Stuut, 2001, chapter 2). Positions of the samples shown in Figs. 2 and 3 are indicated with arrows. (B) $CaCO_3$ (%) record of core GeoB 1028-5 (Schmidt, 1992). (C) Carbonate fragmentation index; (log)-ratio of the relative abundance of the coarsest two modes in the size distributions of bulk sediments from core MD962094. Carbonate fragmentation increases to the left. (D) Foraminifer Fragmentation Index (Schmidt, 1992) constructed from the ratio of fragments of foraminifera shells over whole foraminifera shells in core GeoB 1028-5. Fragmentation increases to the left. (E) Relative wind-strength curve derived from the grain size of eolian dust (Stuut et al., 2002), relative wind strength increases to the left.

boundaries between the individual chambers (G.-J. Brummer, pers. commun., 2001).

6. Application of the carbonate fragmentation index to deep-marine sediments

We have demonstrated that the ratio of the coarsest two modes in grain size distributions of carbonate-rich deep-marine sediments can be used as a proxy for carbonate fragmentation, attributed to carbonate dissolution. The grain size distributions of the carbonate-free sediment fractions do not influence the grain size distributions of the bulk sediment fraction and, therefore, the bulk sediment fraction may be considered representative of the carbonate grain size distributions for sediments that contain $> 68\%$ $CaCO_3$ (carbonate ooze). The size distribution of the carbonate fraction of deep-marine sediments can be calculated by subtraction of the carbonate-free size distribution from the bulk size distribution in the right proportion, given by the carbonate content of the sediments (McCave et al., 1995; Trentesaux et al., 2001). Our carbonate fragmentation index can subsequently be calculated from the size distribution of the carbonate fraction of the sediments. However, this method would be rather time consuming and labor intensive. The advantage of the fast and precise method presented here can only be obtained from deep-sea sediments that are carbonate rich ($CaCO_3 > 68\%$).

7. Conclusion

The fragmentation of the foraminifera shells is caused by the dissolution of carbonate in the water column and on the seafloor. The dissolution is reflected by the size distributions of the foraminifer nannofossil ooze and is described by the ratio of the coarsest two fractions. This ratio, or carbonate fragmentation index, can be constructed in a fast and reproducible way by analyzing the size distribution of bulk carbonate-rich sediments. This method can be applied in other areas in the world's oceans where sediments are carbonate rich ($CaCO_3 > 68\%$).

Acknowledgements

We thank the crew and scientists aboard N.O. *Marion Dufresne* for their help with coring and sampling operations during IMAGES II. Geert-Jan Brummer and George Postma read an earlier version of the manuscript. Jacques Giraudeau and Hervé Chamley are thanked for their helpful suggestions to improve this manuscript. This work was financed by the NSG–NIOZ–Bremen cooperation. This is Netherlands Research School of Sedimentary Geology Publication No. 20 010 305 and NIOZ publication number 3701.

References

Arrhenius, G., 1952. Sediment Cores from the East Pacific. Reports Swedish Deep-Sea Expedition 1947–1948, 5.

Barth, T.F.W., Correns, C.W., Eskola, P., 1939. Die Entstehung der Gesteine: Ein Lehrbuch der Petrogenese. Springer, Berlin, 422 pp.

Bassinot, F.C., Beaufort, L., Vincent, E., Labeyrie, L.D., Rostek, F., Müller, P.J., Quidelleur, X., Lancelot, Y., 1994. Coarse fraction fluctuation in pelagic carbonate sediments from the tropical Indian Ocean: A 1500 kyr record of carbonate dissolution. Paleoceanography 9, 579–600.

Berger, W.H., 1968. Planktonic foraminifera: selective solution and paleoclimatic interpretation. Deep-Sea Res. 15, 31–43.

Berger, W.H., 1970. Planktonic foraminifera: Selective solution and the lysocline. Mar. Geol. 8, 111–138.

Berger, W.H., 1973. Deep-sea carbonates: Pleistocene dissolution cycles. J. Foraminif. Res. 3, 187–195.

Berger, W.H., 1979. Preservation of Foraminifera, SEPM Short Course 6. Society for Sedimentary Geology, Houston, TX, pp. 105–155.

Bertrand, P., Balut, Y., Schneider, R., Chen, M.T., Rogers, J. and shipboard scientific party, 1996. Scientific Report of the NAUSICAA-IMAGES II coring cruise. Université Bordeaux-1, Département de Geologie et Oceanographie, Talence, France.

Bramlette, M.N., 1961. Pelagic sediments. In: Sears, M. (Ed.), Oceanography. American Association for the Advancement of Science Publication 67, pp. 345–366.

Broecker, W.S., Clark, E., 1999. $CaCO_3$ size distribution: A paleocarbonate ion proxy? Paleoceanography 14, 596–604.

Broecker, W.S., Takahashi, T., 1980. Hydrography of the Central Atlantic-III. The North Atlantic deep-water complex. Deep-Sea Res. 27A, 591–613.

Brummer, G.-J.A., Kroon, D., 1988. Planktonic Foraminifers as Tracers of Ocean-Climate History: Ontogeny, Relationships and Preservation of Modern Species and Stable Isotopes, Phenotypes and Assemblage Distribution in Different

Water Masses. Ph.D. Thesis, Vrije Universiteit, Amsterdam, 346 pp.

Conan, S.M.-H., Ivanova, E., Brummer, G.-J.A., 2002. Quantifying carbonate dissolution and calibration of foraminiferal dissolution indices in the Somali Basin. Mar. Geol. 182, 325−349.

Diester-Haaß, L., 1985. Late Quaternary sedimentation on the Eastern Walvis Ridge, SE Atlantic. Mar. Geol. 65, 145–189.

Dittert, N., Henrich, R., 2000. Carbonate dissolution in the South Atlantic Ocean: Evidence from ultrastructure breakdown in *Globigerina bulloides*. Deep-Sea Res. 47, 603–620.

Embley, R.W., Morley, J.J., 1980. Quarternary sedimentation and paleoenvironmental studies off Namibia (SW-Africa). Mar. Geol. 36, 183–204.

Emerson, S., Bender, M., 1981. Carbon fluxes at the sediment-water interface of the deep-sea: Calcium carbonate preservation. J. Mar. Res. 39, 139–162.

Farrell, J.W., Prell, W.L., 1989. Climatic change and $CaCO_3$ preservation: An 800,000 year bathymetric reconstruction from the central equatorial Pacific ocean. Paleoceanography 4, 447–466.

Farrell, J.W., Prell, W.L., 1991. Pacific $CaCO_3$ preservation and $\delta^{18}O$ since 4 Ma: Paleoceanic and paleoclimatic implications. Paleoceanography 6, 485–498.

Fischer, G., Wefer, G. (Eds.), 1999. Use of Proxies in Paleoceanography. Springer, Berlin, 735 pp.

Huber, R., Meggers, H., Baumann, K.-H., R, H., 2000. Recent and Pleistocene carbonate dissolution in sediments of the Norwegian–Greenland Sea. Mar. Geol. 165, 123–136.

Kroon, D., Darling, K., 1995. Size and upwelling control of the stable isotope composition of *Neogloboquadrina dutertrei* (d'Orbigny), *Globigerinoides ruber* (d'Orbigny) and *Globigerina bulloides* (d'Orbigny): Examples from the Panama Basin and Arabian Sea. J. Foraminif. Res. 25, 39–52.

Kucera, M., Malmgren, B.A., Sturesson, U., 1997. Foraminiferal dissolution at shallow depths of the Walvis Ridge and Rio Grand Rise during the latest Cretaceous: Inferences for deep-water circulation in the South Atlantic. Palaeogeogr. Palaeoclimatol. Palaeoecol. 129, 195–212.

Le, J., Shackleton, N.J., 1992. Carbonate dissolution fluctuations in the western equatorial Pacific during the Late Quaternary. Paleoceanography 7, 21–42.

Little, M.G., Schneider, R.R., Kroon, D., Price, B., Summerhayes, C.P., Segl, M., 1997. Trade wind forcing of upwelling, seasonality, and Heinrich events as a response to sub-Milankovitch climate variability. Paleoceanography 12, 568–576.

Lohmann, G.P., Rosenthal, Y., McCorkle, D., 1999. Evidence for changes in ocean carbonate ion concentration and foraminiferal calcite solubility during the last glaciation, AGU Fall meeting. Eos Trans., San Francisco.

McCave, I.N., Manighetti, B., Robinson, S.G., 1995. Sortable silt and fine sediment size/composition slicing: Parameters for palaeocurrent speed and palaeoceanography. Paleoceanography 10, 593–610.

Naidu, P.D., Malmgren, B.A., Bornmalm, L., 1993. Quaternary history of calcium carbonate fluctuations in the western equatorial Indian Ocean (Somali Basin). Palaeogeogr. Palaeoclimatol. Palaeoecol. 103, 21–30.

Parker, F.L., Berger, W.H., 1971. Faunal and solution patterns of planktonic Foraminifera in surface sediments of the South Pacific. Deep-Sea Res. 18, 73–107.

Peeters, F.J.C., Ivanova, E.M., Conan, S.M.-H., Brummer, G.J.A., Ganssen, G.M., Troelstra, S.R., Van Hinte, J.E., 1999. A size analysis of planktic foraminifera from the Arabian Sea. Mar. Micropaleontol. 36, 31–63.

Peterson, L.C., Prell, W.L., 1985a. Carbonate dissolution in recent sediments of the eastern equatorial Indian Ocean: Preservation patterns and carbonate loss above the lysocline. Mar. Geol. 64, 259–290.

Peterson, L.C., Prell, W.L., 1985b. Carbonate preservation and rates of climatic change: An 800 kyr record from the Indian Ocean. In: Sundquist, E., Broecker, W. (Eds.), The Carbon Cycle and Atmospheric CO_2: Natural Variations Archean to Present. Geophys. Monogr. Ser. 32., AGU, Washington, DC, pp. 251–269.

Schmidt, H., 1992. Der Benguelastrom im Bereich des Walfisch-Rückens im Spätquartär. Ph.D. Thesis, Bremen University, Bremen, 172 pp.

Stuut, J.-B.W., 2001. Late Quaternary Southwestern African terrestrial-climate signals in the marine record of Walvis Ridge, SE Atlantic Ocean. Geologica Ultraiectina 212, Ph.D. Thesis, Utrecht University, Utrecht, 128 pp.

Stuut, J.-B.W., Prins, M.A., Schneider, R.R., Weltje, G.J., Jansen, J.H.F., Postma, G., 2002. A 300-kyr record of aridity and wind strength in southwestern Africa: Inferences from grain-size distributions of sediments on Walvis Ridge, SE Atlantic. Mar. Geol. 180, 221–233.

Thunell, R.C., 1976. Optimum index of calcium carbonate dissolution in deep-sea sediments. Geology 4, 525–528.

Trentesaux, A., Recourt, P., Bout-Roumazeilles, V., Tribovillard, N., 2001. Carbonate grain-size distribution in hemipelagic sediment from a laser particle sizer. J. Sediment. Res. 71, 858–862.

Ufkes, E., Jansen, J.H.F., Schneider, R.R., 2000. Anomalous occurrences of *Neogloboquadrina pachyderma* (left) in a 420-ky upwelling record from Walvis Ridge (SE Atlantic). Mar. Micropaleontol. 40, 23–42.

Wefer, G., Berger, W.H., Siedler, G., Webb, D.J. (Eds.), 1996. The South Atlantic, Present and Past Circulation. Springer, Berlin, 644 pp.